Research Article | Vol. 29, No. 10 / 10 May 2021 / Optics Express 15802
Optics EXPRESS

1.3 μm wavelength tunable single-mode laser arrays based on slots

MICHAEL MCDERMOTT,[1,*] ROBERT MCKENNA,[1] CAOLÁN MURPHY,[1] DOVYDAS MICKUS,[1] HAI-ZHONG WENG,[1] SEPIDEH NAIMI,[1] QIAOYIN LU,[2] WEI-HUA GUO,[2] MICHAEL WALLACE,[1] NICOLÁS ABADÍA,[3] AND JOHN F. DONEGAN[1]

[1] *School of Physics, CRANN and AMBER, Trinity College Dublin, Dublin 2, Ireland*
[2] *Wuhan National Laboratory for Optoelectronics, and School of Optical and Electronic Information, Huazhong University of Science and Technology, 1037 Luoyu Road, Wuhan 430074, China*
[3] *School of Physics and Astronomy, Cardiff University, Queen's Buildings, The Parade, Cardiff CF24 3AA, UK Institute for Compound Semiconductors, Cardiff University, Queen's Buildings, The Parade, Cardiff CF24 3AA, UK*
[*] *mcdermm6@tcd.ie*

Abstract: Two twelve-channel arrays based on surface-etched slot gratings, one with non-uniformly spaced slots and another with uniformly spaced slots are presented for laser operation in the O-band. A wavelength tuning range greater than 40 nm, with a side-mode suppression ratio (SMSR) > 40 dB over much of this range and output power greater than 20 mW, was obtained for the array with non-uniform slots over a temperature range of 15 °C - 60 °C. The introduction of multiple slot periods, chosen such that there is minimal overlap among the side reflection peaks, is employed to suppress modes lasing one free spectral range (FSR) from the intended wavelength. The tuning range of the array with uniformly spaced slots, on the other hand, was found to be discontinuous due to mode-hopping to modes one FSR away from the intended lasing mode which are not adequately suppressed. Spectral linewidth was found to vary across devices with the lowest measured linewidths in the range of 2 MHz to 4 MHz.

1. Introduction

Tunable semiconductor lasers are key components for dense-wavelength division multiplexed (DWDM) optical communication systems. DWDM requires a wide wavelength tuning range and narrow spectral linewidth for coherent communication systems. Many types of tunable C-band wavelength sources such as sampled grating DBR (SGDBR) lasers [1], grating-coupled sampled reflector (GCSR) lasers [2], external cavity lasers (ECL) [3] and vertical-cavity surface-emitting (VCSEL) lasers [4] have been developed for DWDM applications. Recently, state-of-the-art single mode distributed feedback (DFB) laser arrays [5,6], distributed-reflector (DR) [7] laser arrays and electro-absorption modulators integrated with DFB lasers (EADFB) arrays [8] have been developed for DWDM in the O-band with tuning ranges greater than 38 nm with side-mode suppression ratio (SMSR) in excess of 40 dB and a spectral linewidth below 300 kHz. Due to the low dispersion of O-band light in fiber, it is used extensively for applications such as high-speed Ethernet transmission. The result of low fiber dispersion is that expensive dispersion-compensation schemes are not required, reducing the cost of such systems. However, all of these devices require complex regrowth steps and high-resolution processing during the fabrication. Our group has previously demonstrated single-mode tunable lasers in the C-band based on slots etched into the surface of a ridge waveguide with a tuning range greater than 36 nm, SMSR above 50 dB and linewidth below 1 MHz [9,10]. Our group has also demonstrated a six-section device based on surface-etched slots which utilise the Vernier tuning effect to produce a tuning range of over 55 nm with SMSR greater than 30 dB [11]. These devices do not require a regrowth step

#425204 https://doi.org/10.1364/OE.425204
Journal © 2021 Received 17 Mar 2021; revised 21 Apr 2021; accepted 24 Apr 2021; published 7 May 2021

Optics EXPRESS

and can be fabricated by standard photolithography, resulting in a potentially greater device yield [12]. Two arrays of slotted lasers with tunable wavelengths in the O-band are presented here. One array is based on devices with uniformly spaced slots while the other features devices where the slots are non-uniformly spaced with three different period spacings. It will be shown that this three-period array gives the best performance in terms of tuning range and SMSR which compares favourably with the previously referenced state-of-the-art devices despite the much less complicated fabrication requirements. The coming decade will see a large increase in the usage of O-band transmitters in communications networks and also in optical sensing applications.

2. Grating design and simulations

A 2-dimensional representation of the ridge waveguide structure is shown in Fig. 1, this structure acts as a Bragg grating. In order to achieve the best performance from each device, the slot parameters such as the slot width (d_w), slot spacing (d_s), slot depth and the number of slots must be optimised. The 2-D scattering matrix method (SMM) is employed to simulate the effect of a specific grating geometry on the reflectivity and transmission of the slots [13]. The optimum parameters were determined by analysing the grating using the 2-D SMM with varying slot parameters and the simulations were performed using the time-domain transfer matrix method (TDTMM), outlined in [14], which was written in the Python coding language, with a basis reflective spectra simulated using the Cavity Modelling Framework (CAMFR) package. A genetic algorithm has since been developed to improve the optimisation process [15].

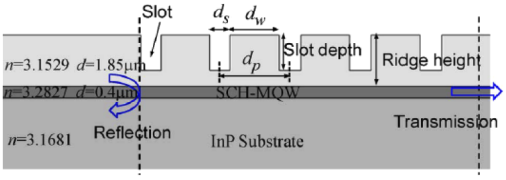

Fig. 1. 2-D waveguide structure featuring slots used to form the laser grating.

Using this method, two 12-channel arrays of high-order slotted surface grating lasers were designed for O-band wavelengths. One array consists of non-uniformly spaced slots, meaning there are slots of more than one period present on the same device, while the second array features devices with a single slot period. Table 1 shows the slot width, period spacing, number of slots and design wavelength of each device. The period order is related to the period length through the Bragg equation:

$$p = \frac{m\lambda_{Bragg}}{2n_{eff}}$$

where p is the grating period length, m is the period order, λ_{Bragg} is the wavelength of the Bragg peak and n_{eff} is the effective index. The arrays are designed such that they span a wavelength range of 40 nm, from 1280 nm to 1320 nm. This is achieved by tuning the periodicity of the slots in the grating section in order to change the centre wavelength. Tuning also refers to the thermal tuning, meaning that the ambient temperature is increased, causing a red-shift in lasing wavelength. The tuning range in this context is the range of wavelengths achieved over the temperature range, from the bluest laser on the array at the lowest temperature to the reddest laser at the highest temperature.

The width of each slot is approximately 1.1 μm, therefore standard photolithography can potentially be used for fabrication. The optimised slot depth is found to be 1.3 μm, the reflectivity increases and the transmission decreases in an exponential fashion with increasing slot depth as described in [16].

Optics EXPRESS

Table 1. *Slot details of each device.*

	Three-Period							Single-Period				
	Width (μm)	Period 1 (μm)	Period 2 (μm)	Period 3 (μm)	#of slots	Wavelength (nm)			Width (μm)	Period (um)	#of slots	Wavelength (nm)
Device 1	1.09	4.75	5.35	5.94	[10, 10, 10]	1280.0		Device 1	1.09	5.15	33	1280.0
Device 2	1.09	4.77	5.36	5.96	[10, 10, 10]	1283.6		Device 2	1.09	5.16	33	1283.6
Device 3	1.10	4.78	5.38	5.97	[10, 10, 10]	1287.3		Device 3	1.10	5.18	33	1287.3
Device 4	1.10	4.79	5.39	5.99	[10, 10, 10]	1290.9		Device 4	1.10	5.19	33	1290.9
Device 5	1.10	4.81	5.41	6.01	[10, 10, 10]	1294.5		Device 5	1.10	5.21	33	1294.5
Device 6	1.11	4.82	5.42	6.03	[10, 10, 10]	1298.2		Device 6	1.31	6.03	23	1298.2
Device 7	1.11	4.83	5.44	6.04	[10, 10, 10]	1301.8		Device 7	1.31	7.86	19	1301.8
Device 8	1.11	4.85	5.45	6.06	[10, 10, 10]	1305.5		Device 8	1.31	6.87	20	1305.5
Device 9	1.12	4.86	5.47	6.08	[10, 10, 10]	1309.1		Device 9	0.91	7.70	17	1309.1
Device 10	1.12	4.87	5.48	6.09	[10, 10, 10]	1312.7		Device 10	1.32	6.70	18	1312.7
Device 11	1.12	4.89	5.50	6.11	[10, 10, 10]	1316.4		Device 11	1.12	5.91	16	1316.4
Device 12	1.12	4.90	5.52	6.13	[10, 10, 10]	1320.0		Device 12	1.12	5.92	16	1320.0

Figure 2 shows the simulated output spectra of the devices using the slot parameters from Table 1 and the corresponding values of the reflectivity and transmission determined by the 2-D SMM along with the TDTMM. Each device on the three-period array, a schematic of which is shown in Fig. 3(a), has a grating section consisting of ten slots of period 1, followed by ten slots of period 2 and then 10 slots of period 3 for a total 30 slots, Fig. 3(b) shows an SEM image of the slots. It has previously been shown in our group that devices based on non-uniformly spaced slots were successful at suppressing modes lasing at one free spectral range (FSR) away from the intended lasing wavelength [10]. This is because, when the periods are chosen such that there is minimal overlap among the side reflection peaks, the side peaks are suppressed and the central mode dominates [17]. The full three-period array is shown in Fig. 3(c). The single-period array consists of devices where slots on each device are equally spaced, but the period order and number of slots differ between the devices. Devices on the blue end of the array feature a greater number of slots in order to better suppress the FSR modes. Although the single period array was designed with 12-channels, Device 12 was not included on this array (instead, it appears that Device 1 had been duplicated) and thus only data for 11 channels of this array are presented here.

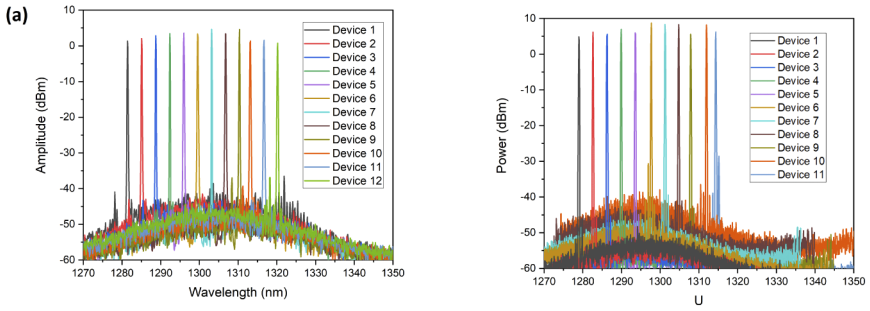

Fig. 2. (a) Three-period simulated output spectrum. (b) Single-period simulated output spectrum.

The simulated spectra show the designed wavelength range of the array, with an average channel spacing of 3.6 nm and a longitudinal mode spacing of approximately 0.65 nm. The simulations indicate that the output power of the single-period array is expected to be higher than that of the three-period array. They also indicate tuning range of approximately 40 nm is to be expected as well as SMSR on the order of 40 dB.

Optics EXPRESS

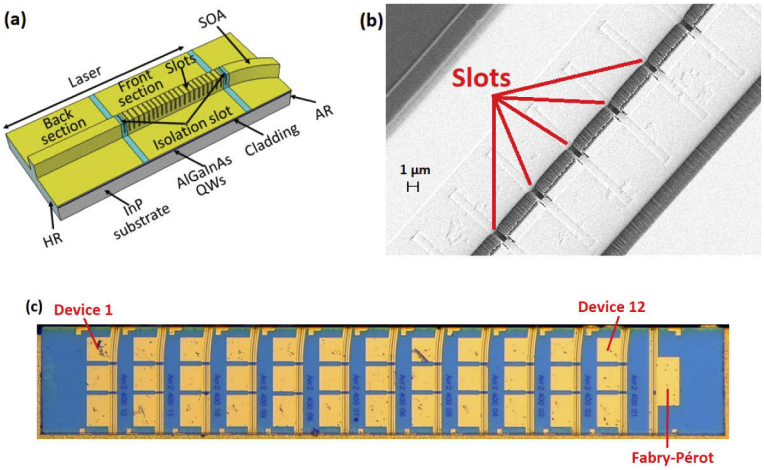

Fig. 3. (a) Device schematic of slotted laser with curved SOA. An anti-reflective (AR) coating is applied to the front facet while a high-reflection (HR) coating is applied to the back facet. The device is mounted on an aluminium nitride carrier which serves as the ground contact. (b) SEM image of device showing the slots. (c) Image of 12-channel array. Device 1 is designed to emit at 1280 nm (blue end) and Device 12 is designed to emit at 1320 nm (red end). Each array also has a Fabry-Perot device with which we can compare the single mode array devices.

3. Device fabrication and structure

Each laser in the array consists of a 2.0 μm-wide surface ridge waveguide with three electrically isolated sections. At the front is a 200 μm long semiconductor optical amplifier (SOA) section, which is curved at a 7^o angle to reduce reflections from the front facet. The middle grating section consists of a number of etched slots, the number and period of which are given in Table 1. The back gain section consists of an active waveguide. The combined length of the gain and grating sections is 400 μm.

There are three contact pads for each laser. The active layer consists of compressively strained AlGaInAs multiple-quantum wells (MQWs) which have an emission peak around 1300 nm. The MQWs consist of five wells of thickness 0.006 μm and six barriers of thickness 0.01 μm. E-beam lithography was used to pattern the slots for this fabrication run due to limitations in the external foundry. Two steps of inductively coupled plasma (ICP) based dry etching with Cl_2 /N_2 gas combinations were used to form the ridge and the slots. First a shallow ridge was formed with the slot area being protected by SiO_2 during the dry etching. Afterwards the protection layer was removed and a second dry etching was used to form the slots and also to etch the ridge to a depth of 1.3 μm. The ridge was then passivated and metal contacted to finish the laser structure. Finally, the laser bars were cleaved and mounted on aluminium nitride carriers.

4. Characterisation

The devices were mounted on a copper heat sink and the temperature was controlled using a thermo-electric cooler (TEC). Thermal wavelength tuning, red-shifting the output wavelength by increasing the ambient temperature, was accomplished by injecting a constant current of 100 mA split across the gain and grating sections such that the current density is equal in both sections, while increasing the temperature from 15 °C - 60 °C in 5 degree increments. A current of 10 mA was injected into the SOA to ensure the section is biased near transparency. The devices were fiber-coupled to an Agilent 86140B optical spectrum analyser (OSA) with a resolution bandwidth

Optics EXPRESS

of 0.06 nm and a sensitivity of -70 dBm. Spectral linewidth was measured using the delayed self-heterodyne (DS-H) method [18].

4.1. L-I characteristic

The light-current (L-I) characteristic of devices on both arrays was performed by sweeping the injected current from 0 mA to 120 mA and measuring the output power using a bare photodiode. Figure 4 shows the light - current (L-I) characteristics of each device. A generally consistent behaviour is seen in both arrays.

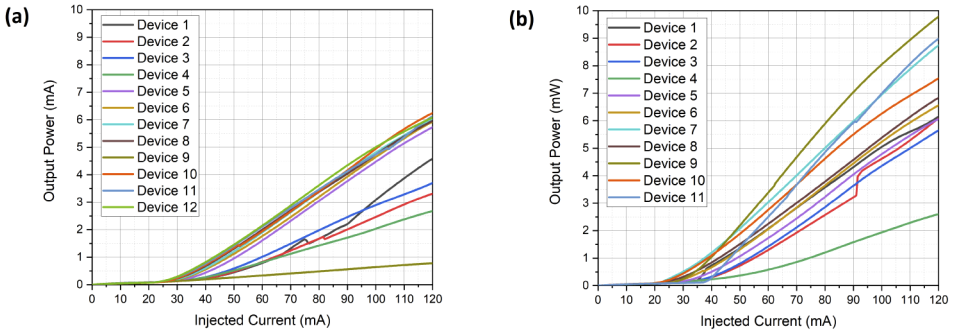

Fig. 4. (a) L-I characteristic of three-period array, Device 9 of this array has noticeably lower output power. (b) L-I characteristic of the single-period array, Device 4 of this array has noticeably lower output power. L-I characterisation was performed at 20 °C with unbiased SOA section.

The threshold current was found to vary from 16 mA to 25 mA for all devices. Device 9 on the three-period array, and Device 4 of the single-period array were found to emit significantly lower output power than the rest of the devices on that array. It is unclear why the output power of this device is so low, there does not appear to be any obvious damage when we observe through the microscope but is likely due to damage such as defects on the facets when cleaving or an error during fabrication. Apart from the aforementioned outliers, the three-period devices show less variation in both threshold and slope efficiency than the single-period devices.

4.2. Output spectra

The output spectra of all devices in each array at 20 °C is presented in Figs. 5(a) and 5(b). The average spacing between modes is approximately 3.3 nm in each array. It was noticed that Devices 1 and 2 of the single-period array emit in the region of 1324 nm and 1327 nm. These devices were designed to emit a wavelength of approximately 1280 nm and 1283 nm respectively. The free spectral range (FSR) of a high-order grating with a slot spacing of 5.15 μm is approximately 47 nm, thus these devices are lasing at a mode one FSR away from the intended wavelength. The three-period devices emit at a wavelength close to the designed wavelength, though blue-shifted by approximately 3 nm from their design. This is the first generation of 1.3 μm devices which have been designed and fabricated by our group. There is clearly room for improvement in future fabrication runs.

There is good agreement between the simulated output spectra shown in Fig. 2 and the experimentally obtained results, although the FSR problem is not as pronounced in the simulations. Gain and refractive index data were not known at the beginning of this work and were therefore estimated from our 1550 nm devices. Now that we are aware of the FSR problem and have better data on the gain and refractive index, we can address these issues when designing the next generation of 1.3 μm devices.

Optics EXPRESS

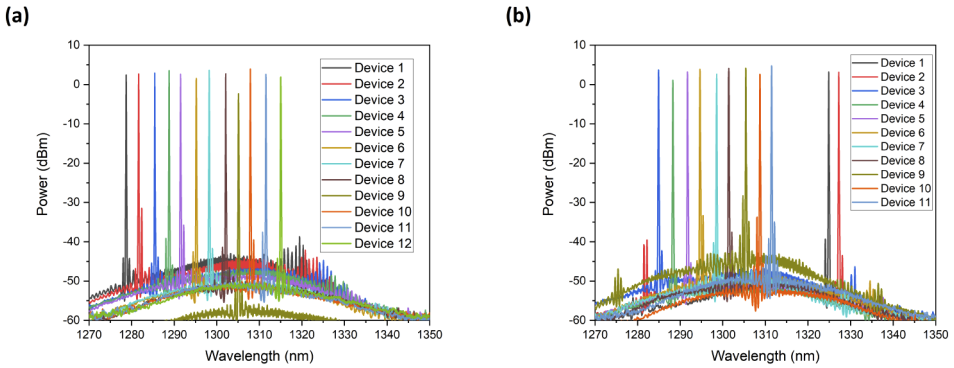

Fig. 5. (a) Three-period experimental output spectrum. (b) Single-period experimental output spectrum.

4.3. Thermal tuning

Figure 6 shows the thermal tuning of both arrays from 15 °C to 60 °C. The output spectrum of each device on the array recorded at 5 degree increments over this temperature range are plotted together to illustrate the wavelength tuning.

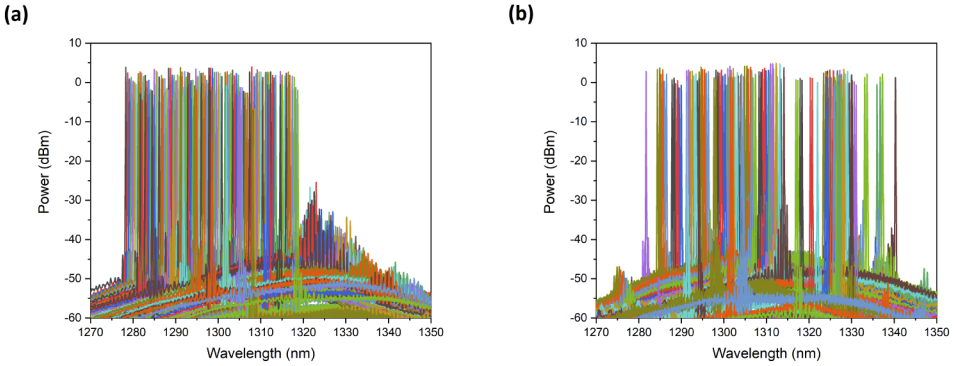

Fig. 6. (a) Three-period array thermal tuning spectra. (b) Single-period array thermal tuning spectra.

The thermal tuning demonstrates a wavelength tuning range of ~40 nm for the three-period array (Fig. 6(a)). However, there are clear discontinuities in the thermal tuning spectrum of the single-period array (Fig. 6(b)) although the range here is up to 60 nm . The plot of wavelength vs temperature for the three-period array (Fig. 7(a)) demonstrates a generally linear red-shift in wavelength of approximately 0.09 nm/°C increase in temperature. In some cases, the wavelength blue-shifts with a temperature increase, due to crossing a mode boundary during tuning. Such mode hops are common in many DBR-type lasers. As temperature increased, it was noticed that the wavelength of the devices on the blue end of the array would reach a point where the emitted wavelength jumped by approximately one FSR, this occurred with 7 devices up to 60 °C. The jumps in wavelength can clearly be seen in Fig. 7(b). Thus, there is not a continuous tuning range for the single-period array. For a majority of the devices, the SMSR is high over this tuning range, above 35 dB as seen in Fig. 7(c). Devices 1 and 2 of this array have comparatively lower SMSR due to the competition from FSR modes in the region of 1320 nm - 1325 nm. We do not observe any jumps to the next FSR due to the suppression of these modes from the use of non-uniformly spaced slots.

Optics EXPRESS

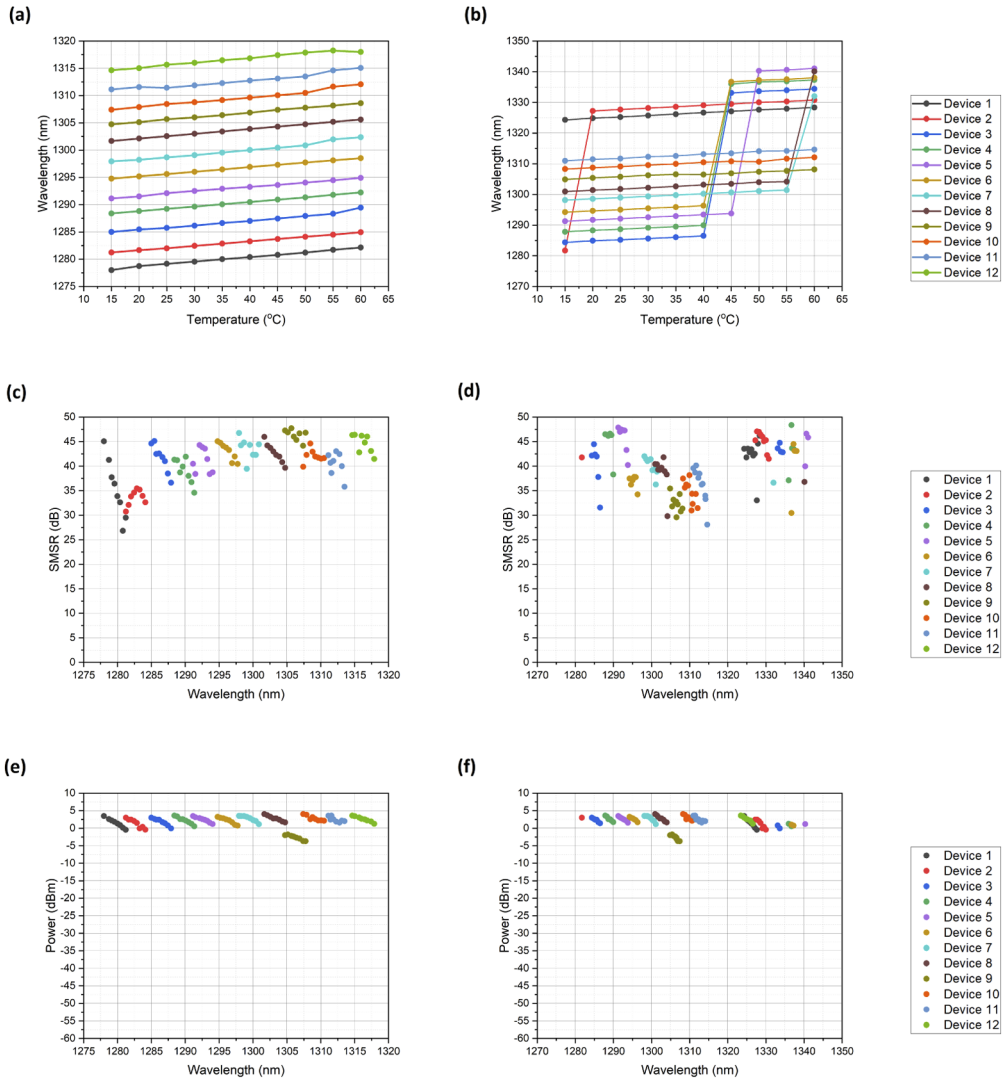

Fig. 7. (a) Three-period array wavelength vs temperature. (b) Single-period array wavelength vs temperature. (c) Three-period array SMSR vs wavelength. (d) Single-period array SMSR vs wavelength. (e) Three-period array power vs wavelength. (f) Single-period array power vs wavelength.

4.4. SOA characterisation

With a constant injection current of 100 mA at 20 °C, the SOA current was increased from 0 mA to 60 mA in increments of 2.5 mA. Figure 8 shows the recorded peak wavelength, SMSR and output power measured for all devices as SOA current was increased.

A red-shifting of the peak wavelength is observed with increasing SOA current and this is especially noticeable at higher SOA currents. Figure 9 shows the peak wavelength and SMSR recorded for Device 12 on both arrays as the SOA current is increased. The red-shifting of the wavelength was found to be 0.6 nm or below for all devices measured over the entire range of SOA currents, or a maximum of 0.01 nm/mA change in SOA current.

Optics EXPRESS

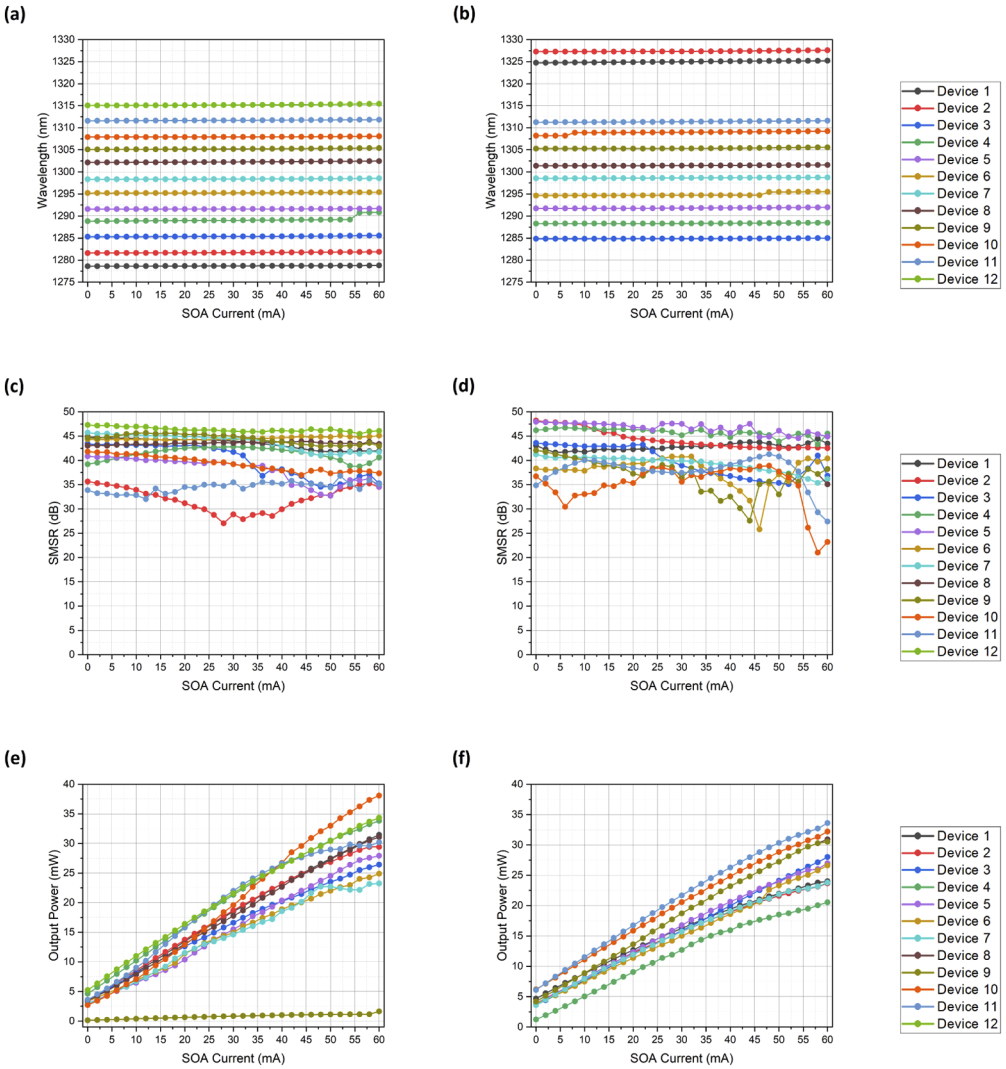

Fig. 8. (a) Three-period wavelength vs SOA current. (b) Single-period wavelength vs SOA current. (c) Three-period SMSR vs SOA current. (d) Single-period SMSR vs SOA current. (e) Three-period power vs SOA current. (f) Single-period power vs SOA current.

Optics EXPRESS

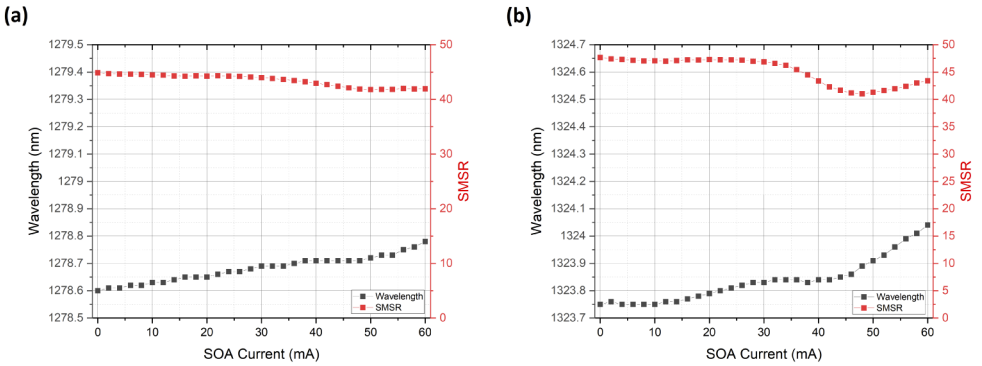

Fig. 9. (a) Three-period array Device 1 SOA characterisation. (b) Single-period array Device 1 SOA characterisation.

SMSR generally remains high for most devices though it can be seen to drop sharply if a mode-hop is approached. With the exception of Device 9 of the three-period array, the increase in output power with SOA current is consistent for devices on the same array. Output powers up to 35 mW are obtained for these devices with this simple SOA section, sufficient for applications in the O-band.

4.5. Linewidth

The spectral linewidth was measured using the delayed self-heterodyne method. Figure 10(b) shows the linewidth spectrum obtained for Device 6 of the three-period array. The data was fitted to a Voigt profile to obtain the Lorentzian full-width at half-maximum (FWHM), which corresponds to the 3 dB linewidth. The FWHM was determined to be 12.6 MHz, indicating a linewidth of 6.3 MHz.

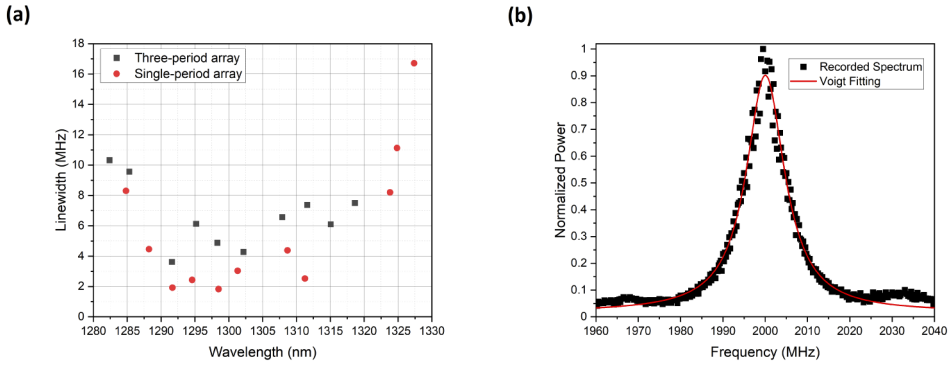

Fig. 10. (a) Linewidth as a function of wavelength. (b) Example linewidth spectrum of Device 6 of the three-period array.

We see the measured linewidth as a function of wavelength in Fig. 10(a). The linewidth enhancement factor increases as the gain peak wavelength is approached, thus we expect the devices lasing at the red end of the array to have the greatest linewidth. This is seen in Fig. 10(a) though we also see relatively large linewidth values at the blue end of the array also. It is likely that, as the modes one FSR away are poorly suppressed in our present designs, this extra noise results in a broader linewidth. Apart from the bluest devices, the measured linewidth generally appears to be broader for the three-period devices. This trend was also observed for the linewidth

Optics EXPRESS

of the 400 μm long devices measured in [10]. Figure 11 shows the output spectrum of Device 3, at the blue of the three-period array, compared to Device 6 which is in the centre of the same array. It can be seen that there is a significant amount of noise from 1325 nm to 1330 nm in the spectrum of Device 3 whereas this is much less prevalent in the spectrum of Device 6. This may explain why, even though the peak wavelength of Device 6 is red-shifted relative to Device 3, the measured linewidth is narrower.

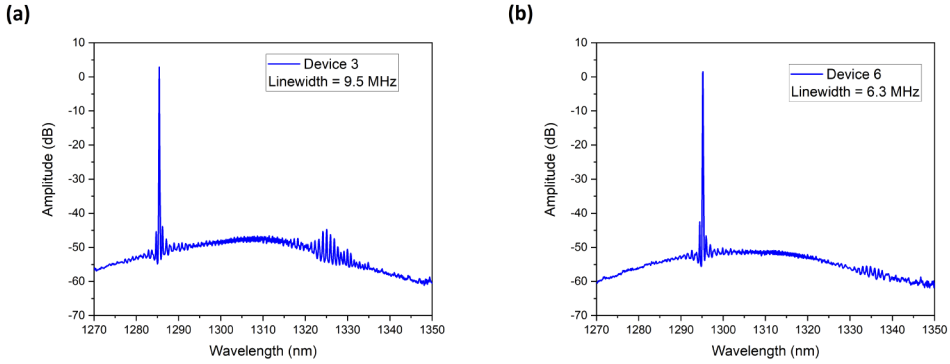

Fig. 11. (a) Optical spectrum of Device 3 of the three-period array. (b) Optical spectrum of Device 6 of the three-period array

5. Conclusion

Both arrays show a consistent L-I characteristic and output power across all devices, with the exception of Device 9 of the three-period array. A continuous thermal tuning range of around 40 nm was obtained for the three-period array with good SMSR (> 35 dB) over the majority of the temperature range. This compares favourably with the eight-device buried heterostructure (BH) DFB array outlined in [6] which demonstrates a continuous tuning range of 38.3 nm with SMSR > 35 dB over the entire tuning range. However, SMSR is poorer at the blue end of our arrays where there is significant competition from the next FSR modes and SMSR drops below 30. This will be improved in future designs by incorporating more slots on the blue end of the array and through the use of the genetic algorithm code to optimize the designs [15]. The output power of the BH DFB devices [6] is in the range of 30 mW - 35 mW at 100 mA injection current, comparable output power can be achieved in many of our devices by increasing the current injected into the SOA section. The single-period devices, with a lower number of slots and a single period, were insufficient to suppress the FSR modes adequately. As a result, devices on the blue end of the array lase at these FSR modes instead of the intended wavelength, and more of the devices make this wavelength jump as the temperature is increased. This resulted in a discontinuous wavelength tuning range. Linewidth was found to vary from 2 MHz for devices in the centre of each array to up to 12 MHz for devices at either end of the array. The linewidth can be improved with designs that suppress the FSR modes. Narrower linewidths can also be achieved by using devices with longer cavity lengths (such as 700 μm and 1 mm) as demonstrated in [10]. In applications where linewidth is not a major consideration, the FSR mode hops could be exploited to increase the tuning range of the array. Overall these results indicate the laser array based on non-uniformly spaced etched slots has great potential for use as a source in O-band DWDM applications due to the tuning range of 40 nm with high SMSR. With a judicious choice of grating designs, it may be possible to use the FSR jumps in a positive fashion to produce a much wider tuning range of 60 nm or more.

Funding. Science Foundation Ireland (15/IA/2854, 17/NSFC/4918).

Optics EXPRESS

Acknowledgements. Microscopy characterisation and analysis has been performed at the CRANN Advanced Microscopy Laboratory (AML www.tcd.ie/crann/aml/).

Disclosures. The authors declare no conflicts of interest.

Data availability. Data underlying the results presented in this paper are not publicly available at this time but may be obtained from the authors upon reasonable request.

References

1. V. Jayaraman, Z.-M. Chuang, and L. A. Coldren, "Theory, design, and performance of extended tuning range semiconductor lasers with sampled gratings," IEEE J. Quantum Electron. **29**(6), 1824–1834 (1993).
2. M. Oberg, S. Nilsson, K. Streubel, J. Wallin, L. Backbom, and T. Klinga, "74 nm wavelength tuning range of an InGaAsP/InP vertical grating assisted codirectional coupler laser with rear sampled grating reflector," IEEE Photonics Technol. Lett. **5**(7), 735–737 (1993).
3. B. Pezeshki, E. Vail, J. Kubicky, G. Yoffe, S. Zou, J. Heanue, P. Epp, S. Rishton, D. Ton, B. Faraji, M. Emanuel, X. Hong, M. Sherback, V. Agrawal, C. Chipman, and T. Razazan, "20-mW widely tunable laser module using DFB array and MEMS selection," IEEE Photonics Technol. Lett. **14**(10), 1457–1459 (2002).
4. K. Knopp, D. Vakhshoori, P. Wang, M. Azimi, M. Jiang, P. Chen, Y. Matsui, K. McCallion, A. Baliga, F. Sakhitab, M. Letsch, B. Johnson, R. Huang, A. Jean, B. DeLargy, C. Pinzone, F. Fan, J. Liu, C. Lu, J. Zhou, H. Zhu, R. Gurjar, P. Tayebati, D. MacDaniel, R. Baorui, R. Waterson, and G. VanderRhodes, "High power MEMs-tunable vertical-cavity surface-emitting lasers," in *2001 Digest of LEOS Summer Topical Meetings: Advanced Semiconductor Lasers and Applications/Ultraviolet and Blue Lasers and Their Applications/Ultralong Haul DWDM Transmission and Networking/WDM Compo*, (IEEE, 2001), pp. 2–pp.
5. L. Lu, Y. Shi, and X. Chen, "Four channel DFB laser array based on the reconstruction-equivalent-chirp technique for 1.3 μm CWDM systems," in *2013 Optical Fiber Communication Conference and Exposition and the National Fiber Optic Engineers Conference (OFC/NFOEC)*, (IEEE, 2013), pp. 1–3.
6. J. Li, S. Tang, J. Wang, Y. Liu, X. Chen, and J. Cheng, "An eight-wavelength BH DFB laser array with equivalent phase shifts for WDM systems," IEEE Photonics Technol. Lett. **26**(16), 1593–1596 (2014).
7. T. Simoyama, M. Matsuda, S. Okumura, A. Uetake, M. Ekawa, and T. Yamamoto, "4-wavelength 25.8-Gbps directly modulated laser array of 1.3-μm AlGaInAs distributed-reflector lasers," in *ISLC 2012 International Semiconductor Laser Conference*, (IEEE, 2012), pp. 54–55.
8. T. Fujisawa, S. Kanazawa, K. Takahata, W. Kobayashi, T. Tadokoro, H. Ishii, and F. Kano, "1.3-μm, 4× 25-Gbit/s, EADFB laser array module with large-output-power and low-driving-voltage for energy-efficient 100GbE transmitter," Opt. Express **20**(1), 614–620 (2012).
9. Q. Lu, W. Guo, A. Abdullaev, M. Nawrocka, J. O'Callaghan, M. Lynch, V. Weldon, and J. F. Donegan, "Tunable single mode laser array based on slots," in *2013 Optical Fiber Communication Conference and Exposition and the National Fiber Optic Engineers Conference (OFC/NFOEC)*, (IEEE, 2013), pp. 1–3.
10. A. Abdullaev, Q. Lu, W. Guo, M. J. Wallace, M. Nawrocka, J. O'Callaghan, and J. F. Donegan, "Improved performance of tunable single mode laser array based on non uniformly spaced slots," in *CLEO: Applications and Technology*, (Optical Society of America, 2015), pp. JTh2A–3.
11. M. Nawrocka, Q. Lu, W.-H. Guo, A. Abdullaev, F. Bello, J. O'Callaghan, T. Cathcart, and J. F. Donegan, "Widely tunable six-section semiconductor laser based on etched slots," Opt. Express **22**(16), 18949–18957 (2014).
12. W.-H. Guo, Q. Lu, M. Nawrocka, A. Abdullaev, J. O'Callaghan, M. Lynch, V. Weldon, and J. F. Donegan, "Integrable slotted single-mode lasers," IEEE Photonics Technol. Lett. **24**(8), 634–636 (2012).
13. Q. Lu, W.-H. Guo, D. Byrne, and J. F. Donegan, "Design of slotted single-mode lasers suitable for photonic integration," IEEE Photonics Technol. Lett. **22**(11), 787–789 (2010).
14. M. Wallace, G. Jain, R. Mckenna, F. Bello, and J. Donegan, "Tuning behaviour of slotted vernier widely tunable lasers," Opt. Express **27**(12), 17122–17137 (2019).
15. M. J. Wallace, S. T. Naimi, G. Jain, R. McKenna, F. Bello, and J. F. Donegan, "Genetic algorithm optimization of high order surface etched grating tunable laser array," Opt. Express **28**(6), 8169–8184 (2020).
16. Q. Y. Lu, W. H. Guo, R. Phelan, D. Byrne, J. F. Donegan, P. Lambkin, and B. Corbett, "Analysis of Slot Characteristics in Slotted Single-Mode Semiconductor Lasers Using the 2-D Scattering Matrix Method," IEEE Photonics Technol. Lett. **18**(24), 2605–2607 (2006).
17. A. Abdullaev, Q. Lu, W. Guo, M. J. Wallace, M. Nawrocka, F. Bello, A. Benson, J. O'Callaghan, and J. F. Donegan, "Improved performance of tunable single-mode laser array based on high-order slotted surface grating," Opt. Express **23**(9), 12072–12078 (2015).
18. T. Okoshi, K. Kikuchi, and A. Nakayama, "Novel method for high resolution measurement of laser output spectrum," Electron. Lett. **16**(16), 630–631 (1980).